

Improving the flotation of ultrafine pyrite in alkaline solution by a novel polystyrene-based nanoparticle collector

Ziyong Chang^{1,2}, Guoyao Li¹, Hao Zhang², Zhengchang Shen³, Laichang Zou¹, Zhongmei Sun¹, Songtao Yang¹

¹ State Key Laboratory of Comprehensive Utilization of Low-Grade Refractory Gold Ores, Zijin Mining Group Co. Ltd., Shang Hang 364200, Fujian;

² Civil and Resource Engineering School, University of Science and Technology Beijing, Beijing, 100083, China;

³ BGRIMM Technology Group, State Key Laboratory of Mineral Processing, Beijing 100160, China.

Corresponding authors: changziyong@ustb.edu.cn (Ziyong Chang), yang_songtao@zijinmining.com (Songtao Yang)

Abstract: It is hard to achieve a satisfactory flotation performance of ultrafine pyrite in alkaline solution using the conventional xanthate collectors. In this work, a novel nanoparticle flotation collector Zijin Nanomaterial (ZJNM) was prepared by emulsion polymerization to enhance the flotation of ultrafine pyrite. It was found that ZJNM was effective in the flotation of ultrafine pyrite with diameter smaller than 18 μm in alkaline solution, which was independent on pH. Mechanism study indicated that the surface of pyrite in alkaline solution was composed of unoxidized surface area and oxidized surface area. ZJNM could adsorb on the unoxidized pyrite surface by forming Fe-S between S atoms on nanoparticles and Fe atoms on pyrite surface, and adsorb on oxidized pyrite surface through hydrogen bonding between $-\text{NH}_2$ on nanoparticles and Fe-OH on pyrite surface, thus increasing the overall hydrophobicity of pyrite and benefit flotation. This work is of guiding significance to enhance the flotation of ultrafine pyrite in practice.

Keywords: flotation, ultrafine pyrite, nanoparticle, collector, adsorption

1. Introduction

In nature, pyrite is often associated with higher valuable metals such as gold, copper, nickel, cobalt and lead (Mohammadi-Jam and Waters 2016). In statistics, almost 85% gold is associated with pyrite (Chen et al. 2014). Hence, it is necessary to concentrate pyrite for the recovery of valuable metals. Froth flotation is well-established and effective in the preconcentration of pyrite, separating valuable minerals from gangue minerals by taking advantage of their difference in surface wettability. In general, a satisfactory flotation performance of pyrite can be achieved in acidic solution when xanthates are used as collectors (Jiang et al. 1998; Niu et al. 2019). However, most flotation tests are conducted in alkaline solution to protect the equipment from being corroded, while the flotation of pyrite is prone to be depressed due to surface oxidation (Yin et al. 2018).

The oxidation of pyrite initiates from crushing, and proceeds with grinding and flotation. In flotation, high pH accelerates pyrite oxidation since OH^- interacts with Fe^{2+} and gives rise to the hydrophilic Fe hydroxides, thereby impeding the adsorption of xanthate collectors and reducing the overall flotation recovery (Yin et al. 2018). In the meantime, with the steady depletion of high-quality mineral resources, the proportion of refractory ores which are characterized of low-grade, finely distributed and miscellaneous is increasing rapidly. For example, carlin type gold deposit is a typical refractory ore that supplies a quarter of the world's gold (Kasymova 2019). Gold is mostly impregnated in pyrite in the form of microscopic and submicroscopic particles, and gold-bearing pyrite is often associated with silicate minerals such as dolomite, quartz and sericite (Hofstra and Cline 2000). As a result, it usually requires fine grinding to obtain sufficient monomer liberation, and a large number of

ultrafine particles below 20 μm are produced, which in turn increased the difficulty of concentrating pyrite by froth flotation.

The development of nanotechnology provides a new approach to effectively recovering fine particles. Nanoparticles are artificially produced microscopic particles no more than 100 nm in diameter, which have been intensively studied in the field of biomedicine (Liu et al. 2024; Abánades Lázaro and Forgan 2019), environmental protection (Chang et al. 2020; Chang et al. 2023), optics (Bharmoria and Ventura 2019; Chang and Wu 2013) and electronics (Jariwala et al. 2013; Tawade et al. 2021). In the past decade (An et al. 2020; Murga et al. 2022; Rahmani et al. 2024; Sobouti et al. 2023), nanoparticles have attracted more and more attention in improving the flotation performance of fine particles. Cilek and Karaca (2015) used nanomaterials as froth stabilizer in mineral flotation to reduce bubble coalescence in froth or bursting on surface, providing a significant increase in barite recovery of 7-11% at deep froth. In addition, the hydrophobic nanoparticles can also be used as flotation collectors to enhance the hydrophobicity of fine particles. Yang et al. (2011) prepared cationic polystyrene nanoparticles by emulsion polymerization, facilitating the attachment of glass bead to air bubbles in flotation. It was found that 5% coverage of the bead surfaces with nanoparticles resulted in high flotation efficiencies. The pull-off force required to pull a glass bead from an air bubble interface into the aqueous phase increased from 0.0086 μN for clean beads to 1.9 μN for glass beads coated with nanoparticles. An et al. (2020) used the hydrophobic polystyrene nanoparticles as a collector for coal flotation, and found that deposition of hydrophobic nanoparticle on coal surfaces increased the hydrophobicity and microscale roughness of coal particles, which was beneficial to flotation process. Murga et al. (2022) used the polystyrene-based nanoparticles St-CTAB and St-CTAB-VI as collectors for chalcopyrite flotation, and found that nanoparticles functionalized by the imidazole group (St-CTAB-VI) achieved better flotation performance.

In this paper, a novel polystyrene-based nanoparticle ZJNM was used to enhance the flotation of ultrafine pyrite in alkaline solution. Mechanisms underpinning the adsorption of ZJNM on pyrite surface were comprehensively investigated through flotation tests and surface analysis. Research findings not only benefit the industry to improve the flotation of ultrafine pyrite in practice, but also pinpoint the research direction of developing novel nanoparticle flotation collectors.

2. Materials and methods

2.1. Materials

Pyrite sample used in this work was obtained from Guangxi Province, China. After handpicking, grinding and screening, mineral particles with diameter smaller than 18 μm were selected for micro-flotation tests and surface characterization. The X-ray diffraction (XRD) pattern of pyrite sample was shown in Fig. 1. As can be seen, the XRD pattern of pyrite sample used in this work is highly consistent with the simulated pyrite sample. And the peaks at 2θ of 28.52°, 33.04°, 37.08°, 40.76°, 47.42° and 56.26° are corresponded to planes of (1 1 1), (2 0 0), (2 1 0), (2 1 1), (2 2 0) and (3 1 1), respectively, indicating that the pyrite sample was of high purity and can be used as pure sample for the respective experimental analysis. Chemicals used in the preparation of nanoparticles such as styrene (99%), 1-allyl-2-thiourea (99%), 2, 2'-azobis (2-methylpropionamide) dihydrochloride (V50, 97%), cetyltrimethylammonium bromide (CTAB, 95%) were purchased from Sigma-Aldrich. Styrene was purified by vacuum distillation, and other reagents were used as supplied. And the reagents used in micro-flotation test, including Y-89 ($\text{C}_6\text{H}_{13}\text{OCSSNa}$), sodium butyl xanthate (SBX) and terpeneol were of industrial grade.

2.2. Methodology

2.2.1. Preparation of nanoparticles

The poly(styrene-co-1-allyl-2-thiourea) based nanoparticle collectors, which was designated as ZJNM, were prepared by emulsion polymerization using a starved-feed semi-batch approach. The comonomer 1-allyl-2-thiourea was designed to functionalize the nanoparticle surface leading to an increased pyrite affinity. The chemical reaction was shown in equation 1. Details of nanoparticle preparation are available in Yang's publications (Yang et al. 2011; Yang and Pelton 2011; Yang et al. 2012).

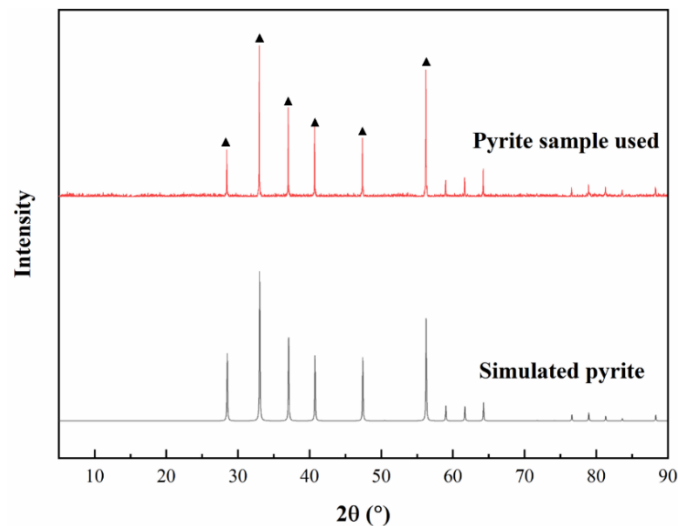
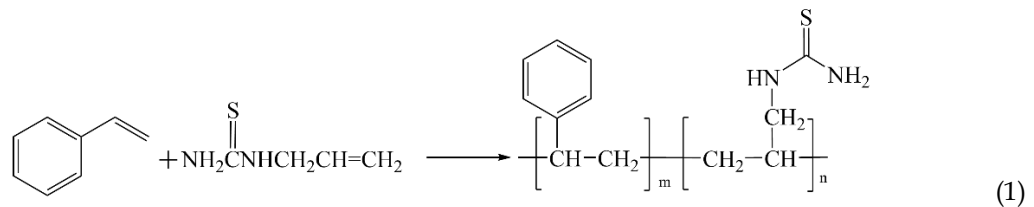


Fig. 1. XRD patterns of pyrite sample



2.2.2. Micro-flotation tests

The single mineral micro-flotation tests were conducted in an XFG flotation cell. For each test, 2g pyrite samples with diameter smaller than 18 μm were mixed with 40 mL de-ionized (DI) water under vigorous agitation. The pH of slurry was regulated to the desired value using 0.1 mol/L HCl and NaOH solution. Collectors and frothers (terpineol, 40 mg/L) were dosed in sequence, and each agent was conditioned for 1 min after addition. The foam products were collected using a scraper for 5 min with collection interval being 6 seconds as concentrates, while the bottom products left in the tank were treated as tailings. Both concentrates and tailings were filtered, dried and weighed to calculate the flotation recovery as equation 2:

$$R = \frac{m_{\text{con}}}{m_{\text{con}} + m_{\text{tail}}} \times 100\% \quad (2)$$

where R (%) is the flotation recovery of pyrite, m_{con} (g) and m_{tail} (g) represent the mass of concentrates and tailings, respectively.

2.2.3. Zeta potential measurement

The zeta potential of pyrite sample was measured using the Bettersizer NS-90Z. For each measurement, 0.1 g pyrite was added to 50 mL DI water with or without flotation reagents. The pH of slurry was adjusted using 0.1 mol/L HCl and NaOH solution to the desired value. After conditioning for 15 min, the slurry was settled for another 15 min and the supernatant was adopted for the zeta potential measurement. Each test was repeated three times to get an average value.

2.2.4. X-ray photoelectron spectroscopy (XPS) analysis

In this work, the interaction between minerals and reagents was investigated using XPS. 2 g samples were ground to below 5 μm before adding to 40 mL DI water, followed by the dosing of flotation reagents at a proper concentration. 0.1 mol/L HCl and 0.1 mol/L NaOH solution were used to adjust the pH to a desired value. After conditioning for 15 min, the samples were filtered and washed with DI water for three times to remove the residual reagents, followed by drying in a vacuum oven at 40 $^{\circ}\text{C}$ overnight. The treated samples were measured using Axis Ultra DLD Kratos Axis Supra with a

monochromatic Al X-ray source operating at 15 kV and 10 mA (150 W). The analysis spot size was 300×700 μm. The binding energy of C 1s at 284.80 eV was used to calibrate the spectrometer.

2.2.5. UV-vis analysis

In this work, the adsorption amounts of Y-89 on pyrite were determined using the ultraviolet spectroscopy. Initially 0.1 g mineral sample and 40 mL DI water were mixed vigorously and regulated to pH 8, followed by the addition of flotation reagents. After a further stirring of 15 min, the suspension was centrifuged at 10000 rpm to achieve a solid-liquid separation. And the supernatant was subject to the UV-vis spectroscopy to determine the residual concentration of Y-89. The adsorption capacity of Y-89 was calculated using equation 3:

$$\Gamma = \frac{(C_0 - C_e)V}{m} \quad (3)$$

where Γ (mol/g) is the adsorption capacity of Y-89, C_0 and C_e (mol/L) denote the initial and residual concentration of Y-89, V (L) is the volume of solution and m (g) is the mass of the sample.

2.2.6. SEM analysis

To gain a vivid presentation of the nanoparticle deposition on pyrite surface, images of the flotation concentrates and tailings using nanoparticle as collector were acquired using the Thermo Scientific Apreo 2 filed emission scanning electron microscopy (SEM). The accelerating voltage used in the test is 5-10 kV, and the amplification factor is 20,000 to 200,000 times.

3. Results and discussion

3.1. Characterization of nanoparticles

In this work, the physicochemical properties of ZJNM used were systematically studied before investigating its effects on the flotation of ultrafine pyrite. As shown in Fig. 2a, the nanoparticles synthesized in this work were irregular spherical particles with a diameter ranging from 100 to 200 nm, and they were prone to agglomerate in aqueous solution. The particle size distribution (PSD) of nanoparticles determined by dynamic light scattering (DLS) showed that two peaks appeared at 47.67 nm and 285.58 nm (Fig. 2b), suggesting that the size distribution of ZJNM was not uniform and aggregation occurred in the aqueous solution. After calculation, the average diameter of ZJNM was around 125 nm, which was consistent with SEM image. Fig. 2c gives the molecular weight distribution of ZJNM determined by gel permeation chromatography (GPC). It can be seen that the molecular weight peaked around 30,000 Dalton, and the average molecular weight was determined to be 30317 Dalton after further calculation. The results confirmed that ZJNM was a macropolymer and the emulsion polymerization reaction was successful. Fig. 1d is the FTIR spectroscopy of ZJNM. The peak at 3483 cm^{-1} represented the -NH stretching vibration peak, and the peak at 2920 cm^{-1} was attributed to the stretching vibration peak of -CH₂. The peak at 1640 cm^{-1} represented the stretching vibration of C=C in benzene ring, coming from polystyrene used in synthesis. The peak at 1400 cm^{-1} was ascribed to the stretching vibration of C-N, which was from the amino groups. Moreover, the peak at 1103 cm^{-1} was the C=S stretching vibration peak. The FTIR spectroscopy indicated that the existence of -NH, -CH₂, benzene ring, C-N, and C=S in the molecular structure of ZJNM, which was consistent with the chemical composition of nanoparticles shown in equation 1.

3.2. Effects of nanoparticle on the flotation of ultrafine pyrite

pH usually plays a significant role in flotation since it can alter the properties of mineral surface and their interaction with flotation reagents. Fig. 3a shows the flotation recovery of ultrafine pyrite as a function of pH in the range of 2-10, when xanthates were used as collectors. As can be seen, when SBX was used as collector, the flotation recovery of pyrite peaked at pH 3.6 with a maximum recovery of 76.7%. Then the recovery dropped sharply at higher pH and only 5.2% pyrite was recovered at pH 8.5, which could be attributed to the entrainment by rising water flow (Wang et al. 2015). The results suggested that pyrite was significantly depressed in alkaline solution with SBX as collector. The flotation curve when Y-89 was used as collector displayed the similar shape, which is consistent with

literature (Lin et al. 2022). Fig. 3b gives the flotation recovery of pyrite as a function of xanthate collector concentration. As can be seen, the recovery of pyrite initially increased with an increase in the concentration of collectors, and a maximum flotation recovery was obtained at 2.0×10^{-4} mol/L, then the flotation recovery decreased gradually with a further increase of collector concentration. Obviously, Y-89 was more effective collector than SBX, indicated by the higher flotation recovery at the same collector concentration. However, the maximum recovery achieved by Y-89 was just 15.19%, suggesting that it was unable to achieve a satisfactory flotation performance of ultrafine pyrite in alkaline solution by increasing the dosage of xanthate collectors only.

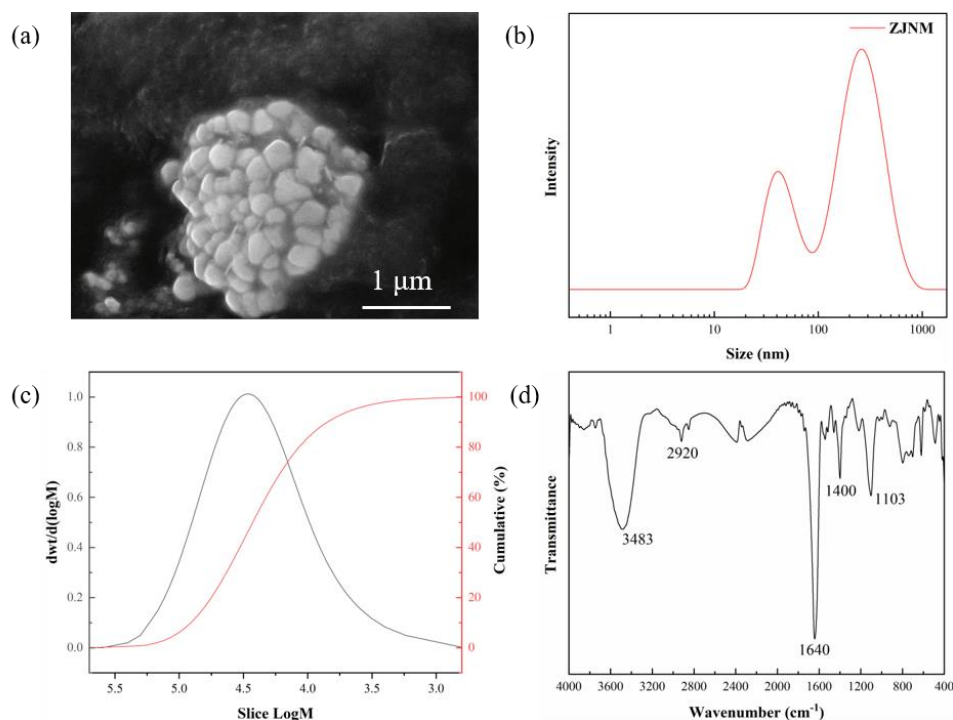


Fig. 2. Characterization of nanoparticle collector: (a) SEM image, (b) particle size distribution, (c) molecular weight distribution, (d) FTIR spectroscopy

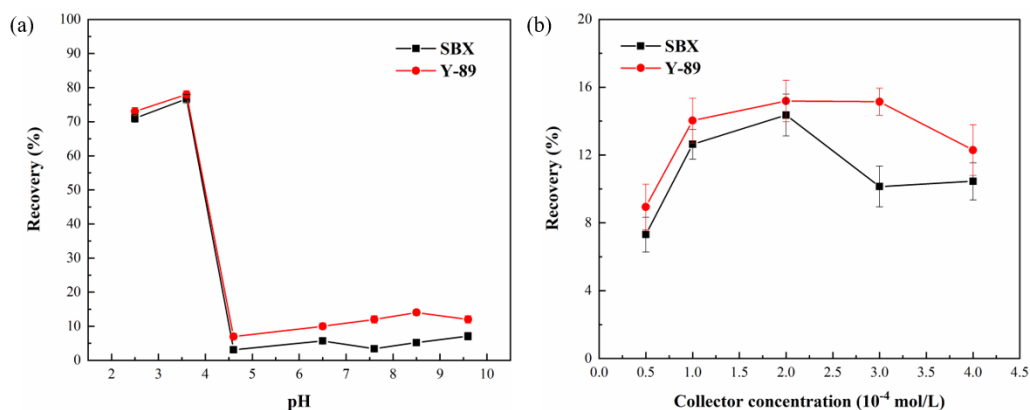


Fig. 3. (a) Effects of pH on the recovery of ultrafine pyrite using SBX and Y-89 as collectors ($C_{\text{SBX}} = C_{\text{Y-89}} = 1.0 \times 10^{-4}$ mol/L); (b) Effects of collector concentration on the flotation recovery of ultrafine pyrite (pH=8.3)

Fig. 4a gives the flotation recovery of ultrafine pyrite as a function of pH when ZJNM was used as collector. As can be seen, the recovery of pyrite remained above 50% in the pH range of 2~10, with only slight fluctuation. The results suggest that the collecting ability of ZJNM for ultrafine pyrite was independent on pH. It is worth noting that the recovery of pyrite reached 60.44% at pH 8.3, which was much higher than that when xanthates were used as collectors, suggesting that ZJNM was much more effective for ultrafine pyrite than xanthate collectors in alkaline solution. Fig. 4b shows the flotation

recovery of pyrite as a function of ZJNM concentration at pH 8.3. Clearly, the flotation recovery of pyrite was positively correlated to the concentration of ZJNM. The flotation recovery of pyrite increased from 34.19% to 60.55% as the concentration of ZJNM increased from 25 mg/L to 100 mg/L.

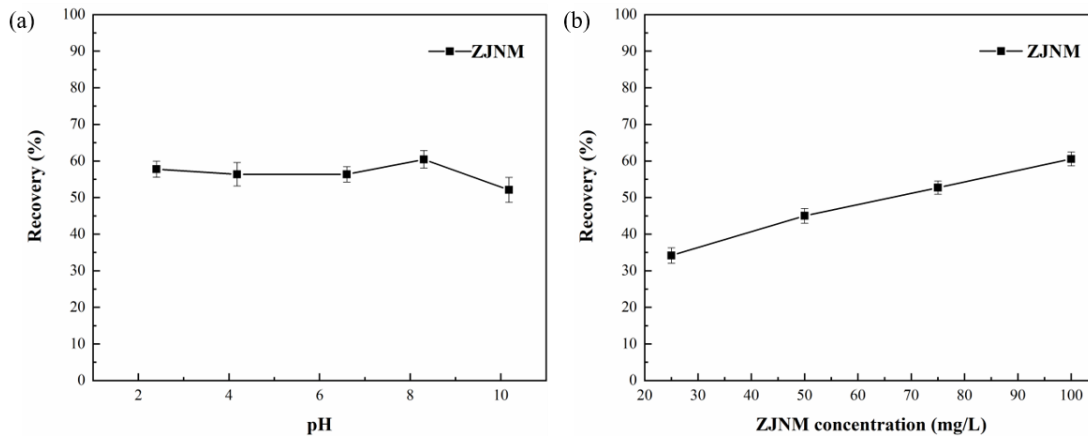


Fig. 4. (a) Effects of pH on the recovery of ultrafine pyrite using ZJNM as collectors (C_{ZJNM} : 100 mg/L); (b) Effects of ZJNM concentration on the flotation recovery of ultrafine pyrite

3.3. Mechanism study

3.3.1. SEM analysis

Fig. 5 shows the SEM images of the concentrate and tailing surfaces when ZJNM was used as the collector. Clearly, the concentrate surface had a high coverage of nanoparticles while the nanoparticle density on tailing surface was much smaller. The nanoparticles on concentrate surface were randomly distributed and some of them aggregated into clusters, which could increase the surface roughness and benefit mineral flotation. As reported by the previous researchers, the microscale roughness of mineral surface could increase the contact angle, thus promoting the attachment efficiency of particle-to-bubble (An et al. 2020; Vaziri Hassas et al. 2016).

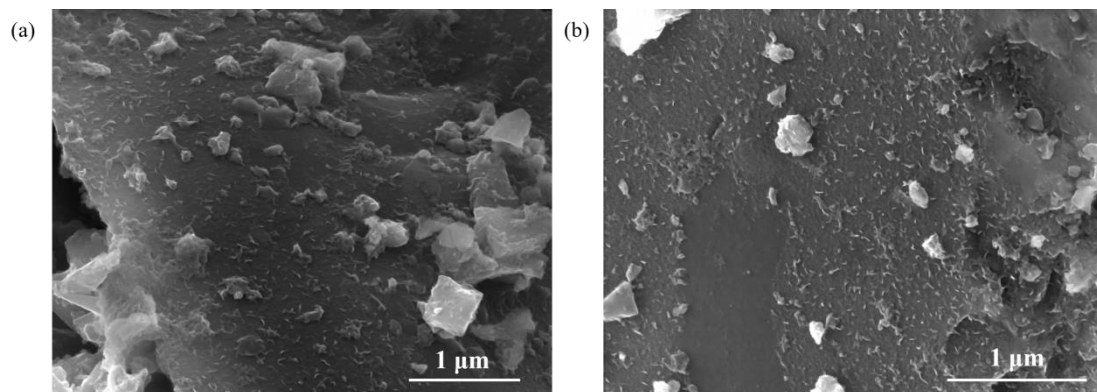


Fig. 5. SEM images of flotation products using nanoparticle as collectors: (a) concentrates, (b) tailings

3.3.2. Zeta potential measurement

Zeta potential is an important indicator to assess the electronic properties of minerals, and it is also frequently used to study the interaction between flotation reagents and mineral surface. Fig. 6 shows the Zeta potential of pyrite in the pH range of 2~11 with and without conditioning with ZJNM and Y-89. In general, the zeta potential of pyrite was positive at low pH, then decreased to zero and converted to be negative with an increase in pH. As shown in Fig. 6, the isoelectric point (IEP) of pure pyrite without the addition of ZJNM was around 6.46, which is close to the value reported by Gaudin and Sun (Sun 1946). After conditioning with Y-89 and ZJNM, the IEP was negatively shifted to 5.39 and 5.70, respectively, and the zeta potential of pyrite at each pH was reduced to some extent. It is noteworthy

that, at pH around 8, the zeta potential decreased from -7.3 mV for pyrite to -8.34 mV for pyrite+Y-89 and -19.6 mV for pyrite + ZJNM, with a decrease of Zeta potential by 1.04 mV and 12.3 mV, suggesting that ZJNM had a stronger affinity for pyrite in alkaline solution than Y-89.

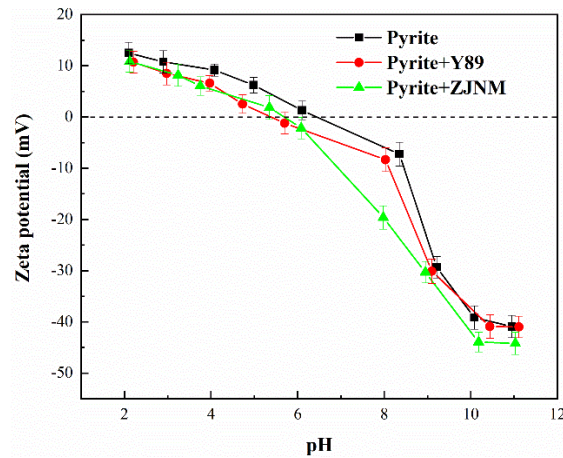


Fig. 6. Effects of pH on the zeta potential of ultrafine pyrite

3.3.3. UV-vis analysis

UV-vis spectroscopy is one of the most popular analytical techniques to determine the concentration of molecules in solution, which is positively correlated to the absorbance intensity. Fig. 7a shows the UV-vis spectrum of ZJNM and Y-89 in the wavelength of 200-400 nm. As can be seen, the characteristic peak of Y-89 appeared at a wavelength of 300 nm, while no peak was detected at 300 nm for ZJNM. Therefore, the absorbance intensity at 300 nm could be used to assess the concentration of Y-89 when both agents were used. Fig. 7b shows the UV-vis absorbance spectrum of Y-89 treated by pyrite and ZJNM. Without the addition of ZJNM, the peak intensity of Y-89 decreased significantly after treating with pyrite, suggesting that Y-89 could still adsorb on pyrite surface. This is because although ultrafine pyrite is easy to get oxidized in alkaline solution, there is still unoxidized pyrite surface which could offer adsorption sites for xanthates. Upon the addition of ZJNM, the peak intensity at 300 nm increased sharply, almost equal to the peak intensity of Y-89 only, indicating that the presence of ZJNM decreased the adsorption of Y-89 on pyrite. In other words, ZJNM exhibited a stronger affinity for pyrite than Y-89 in alkaline solution, which is consistent with flotation and Zeta potential measurement results.

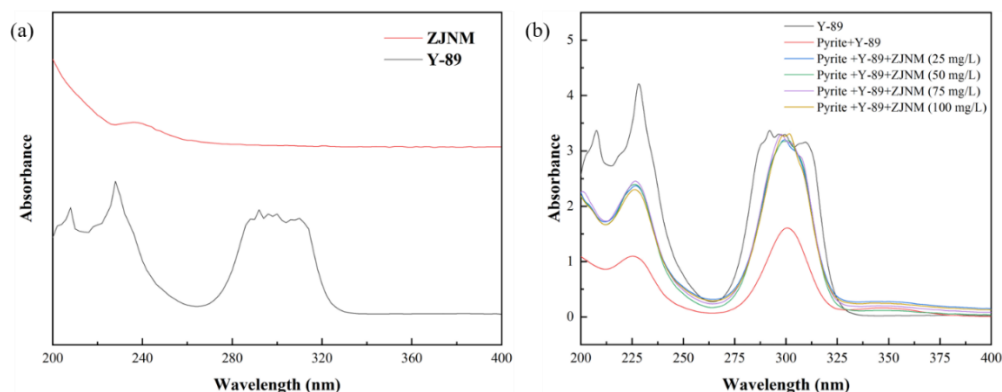


Fig. 7. (a) The UV-vis spectrum of ZJNM and Y-89 without treating with pyrite; (b) Effects of ZJNM on the UV-vis spectrum of Y-89 treated with pyrite (Y-89: 1×10^{-4} mol/L, pH=8.3)

3.3.4. XPS analysis

To gain a deep insight into the interaction between pyrite and ZJNM, the XPS survey scan and high-resolution scan of characteristic elements (Fe, S and N) of pyrite with and without ZJNM were conducted, and the relative elemental composition was summarized to investigate the changes in chemical properties of pyrite surface.

The survey spectrum (Fig. 8a) revealed that the surface of pristine pyrite was composed of Fe, O, C and S, of which C mainly comes from carbon pollution introduced during the test and the presence of O suggested that pyrite surface was oxidized in alkaline solution (Ekmekçi and Demirel 1997; Niu et al. 2019). A new peak indexed to N 1s emerged after treating by ZJNM, suggesting that ZJNM adsorbed on pyrite surface. Fig. 8b gives the elemental composition of pyrite surface before and after treating by ZJNM. Specifically, after treating by 100 mg/L ZJNM, the concentration of C increased to 35.61%, while the concentration of O, Fe and S decreased to 47.76%, 7.60% and 7.56%, respectively. The concentration of N increased from 0.00% to 1.47%. This is because the adsorption of ZJNM on pyrite surface increased the content of C, N and the total amount of surface elements, resulting in the changes of the relative content of each component.

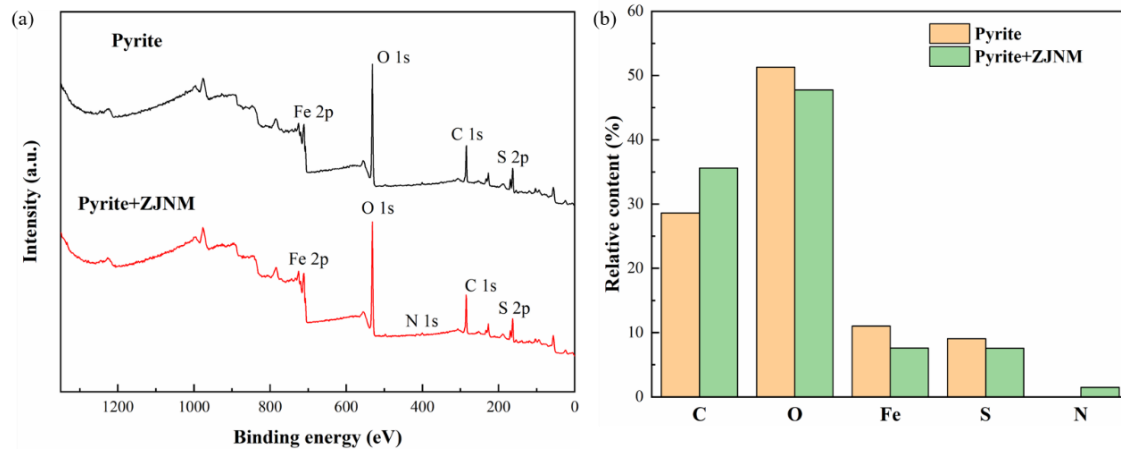


Fig. 8. (a) The XPS survey scan and (b) elemental composition of pyrite surface with and without treating by ZJNM

Fig. 9a is the high-resolution scan of Fe 2p on pyrite surface before and after treating by ZJNM, and Fig. 10a is the corresponding analysis results of Fe species. In general, six peaks emerged in the Fe 2p spectra of pristine pyrite surface without treating by ZJNM, which were attributed to Fe (II)-S at 707.10 eV, Fe (III)-S at 708.67 eV, Fe (II)-O at 710.21 eV and Fe (III)-O at 711.32 eV, 712.63 eV and 714.62 eV (Li et al. 2019), respectively. The presence of Fe (II)-O and Fe (III)-O indicated that pyrite oxidized in alkaline solution and form Fe hydroxides, which is consistent with the survey scan results. It is noteworthy that surface oxidation impeded the adsorption of Y-89 on pyrite, resulting in the low flotation efficiency. Similar peaks can also be found in the deconvoluted Fe 2p spectra of pyrite after treating by ZJNM. Compared to pristine pyrite, the relative concentration of Fe (II)-S and Fe (III)-S on pyrite surface increased obviously after treating by ZJNM, implying that ZJNM could adsorb on pyrite surface by forming Fe-S bond. Furthermore, the binding energy of Fe (II)-O shifted from 710.21 eV to 710.11 eV, and the binding energy of Fe (III)-O shifted from 711.32 eV, 712.63 eV and 714.62 eV for pristine pyrite to 711.13 eV, 712.36 eV and 714.01 eV after treating by ZJNM, demonstrating that Fe-OH on oxidized pyrite surface interacted with $-NH_2$ of nanoparticle through hydrogen bonding. Therefore, it could be concluded that ZJNM could adsorb on both the unoxidized pyrite surface area and oxidized pyrite surface area.

Fig. 9b is the high-resolution scan of S 2p on pyrite surface before and after treating by ZJNM, and Fig. 10b is the corresponding relative concentration of S species. Before treating by ZJNM, the S 2p spectra can be further deconvoluted into S^{2-} at 161.88 eV, S_2^{2-} at 162.72 eV, S_n^{2-} at 163.88 eV, SO_3^{2-} at 165.48 eV and SO_4^{2-} at 168.88 eV (Shen et al. 2019; Zhang et al. 2022). The existence of SO_3^{2-} and SO_4^{2-} suggests that sulfates and sulfites are generated as a result of pyrite oxidation in alkaline solution, which is consistent with literature (Ekmekçi and Demirel 1997; Niu et al. 2019). Additionally, after treating by ZJNM, a new peak representing C-S emerged at 164.3 eV, which may be converted from C=S during the interaction between ZJNM and pyrite. Moreover, as revealed by Fig. 10b, compared to pristine pyrite, the relative concentration of S^{2-} and S_2^{2-} increased after treating by ZJNM. Therefore, both the high-resolution scan of Fe 2p and S 2p confirmed that ZJNM could be adsorbed on pyrite surface in alkaline solution by forming Fe-S bond.

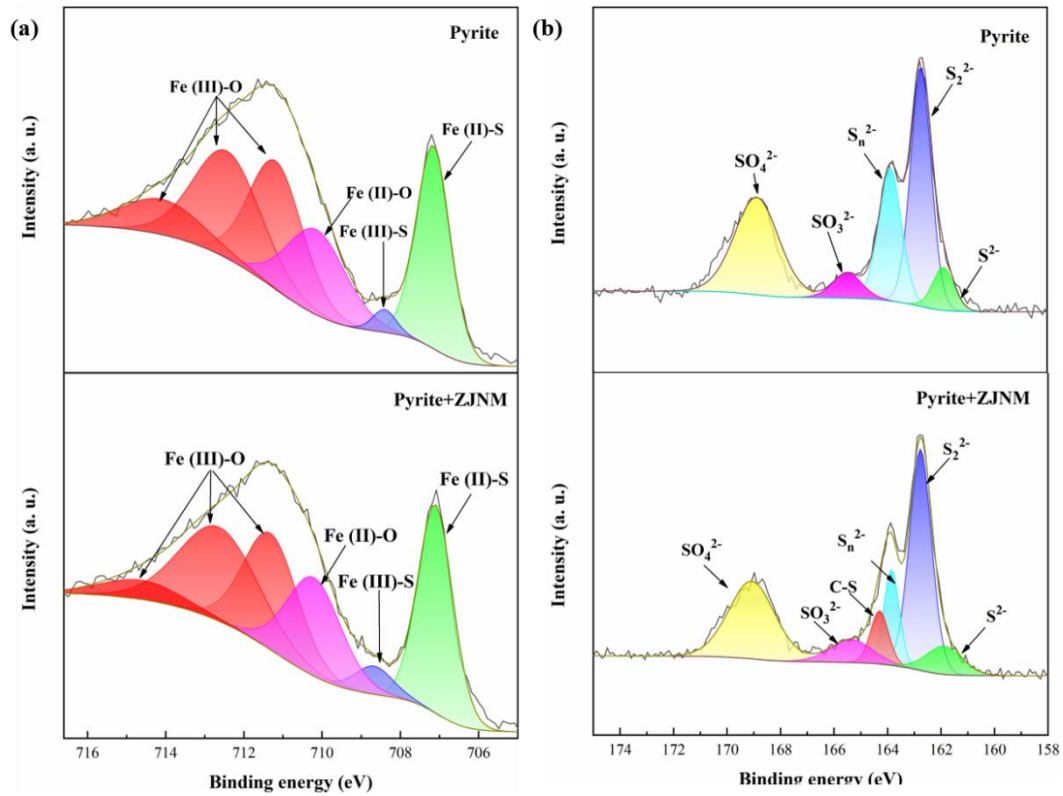


Fig. 9. The high-resolution scan of characteristic elements of pyrite before and after treating by ZJNM: (a) Fe 2p, (b) S 2p

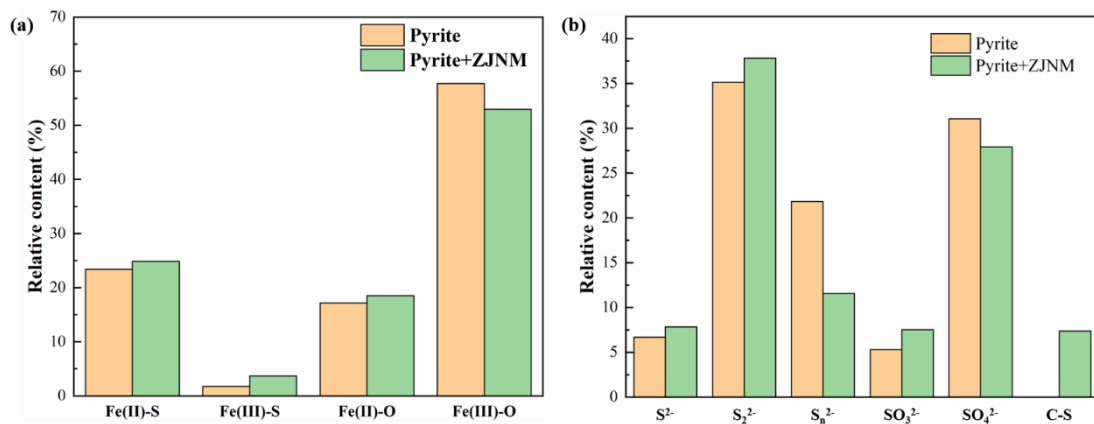


Fig.10. The relative content of Fe and S on pyrite surface before and after treating by ZJNM: (a) Fe, (b) S

Fig. 11 is the XPS spectra of N 1s and the relative content of N on pyrite surface after treating by ZJNM. As shown in Fig. 11a, the N 1s spectra were further deconvoluted into three peaks including C-N at 399.68 eV, N-H at 401.08 eV, and N-O at 402.28 eV (Riedo et al. 2000; Chang et al. 2023), respectively. And the corresponding relative content of N species was 35.67%, 42.38% and 21.95% (Fig. 11b). C-N and N-H were from the thiourea groups of ZJNM, and the presence of N-O indicated that ZJNM adsorbed on the oxidized pyrite surface through the interaction between N atoms of nanoparticles and O atoms of pyrite surface, which is consistent with the analysis results of Fe 2p. This can account for the stronger binding affinity of ZJNM towards pyrite in alkaline solution than Y-89.

Above all, based on the flotation tests and surface analysis results, the interaction between ZJNM and pyrite surface in alkaline solution can be drawn. Pyrite is easy to get oxidized in alkaline solution and is composed of oxidized surface area and unoxidized surface area. On the unoxidized surface area, ZJNM adsorbed through the interaction between S atoms on nanoparticles and Fe atoms on pyrite

surface, and the hydrocarbon chains were oriented outwards to enhance the surface hydrophobicity. On the oxidized surface area, ZJNM adsorbed through the interaction between N atoms on nanoparticles and Fe-OH on pyrite surface, and the hydrophobicity can also be increased by the hydrocarbon chains. As a comparison, the xanthate collector Y-89 could only adsorb on the unoxidized surface area. Therefore, ZJNM possessed a stronger binding affinity towards pyrite in alkaline solution than Y-89 and resulted in superior flotation performance.

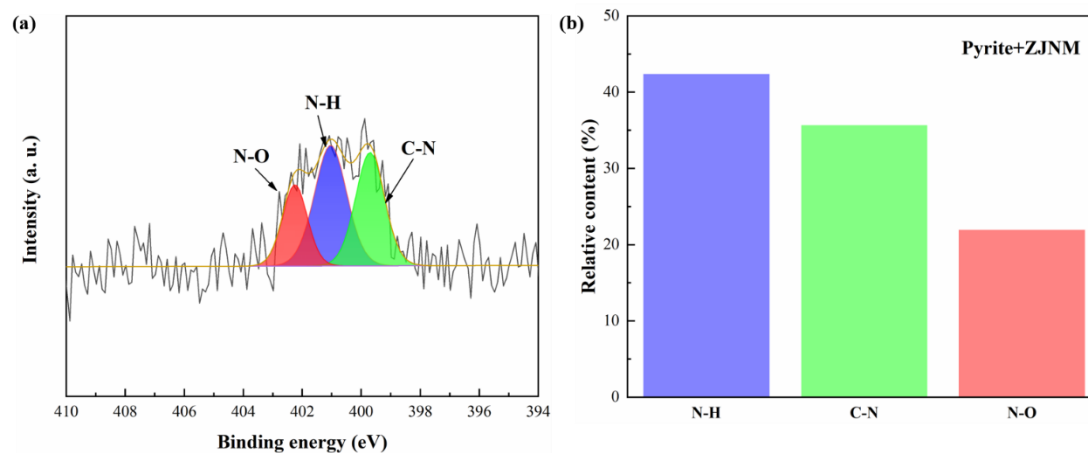


Fig. 11. (a) The high-resolution scan of N 1s and (b) relative content of N on pyrite surface after treating by ZJNM

4. Conclusions

In this work, a polystyrene based hydrophobic nanoparticle collector ZJNM, with an average diameter around 125 nm, was prepared by emulsion polymerization and used to enhance the flotation of ultrafine pyrite. The underlying mechanisms were investigated through SEM imaging, zeta potential measurement, UV-vis spectrum and XPS analysis. It was found that the flotation performance of ultrafine pyrite with xanthate collector SBX and Y-89 was highly dependent on pH, and xanthate collector was unable to achieve a satisfactory flotation performance of ultrafine pyrite in alkaline solution. As a comparison, the nanoparticle collector ZJNM was effective in the flotation of ultrafine pyrite, which was independent on pH. Mechanism study demonstrated that ZJNM selectively deposited on the concentrate surface, and exhibited stronger binding affinity towards pyrite in alkaline solution than Y-89. The XPS analysis results indicated that, the surface of pyrite in alkaline solution was composed of unoxidized surface area and oxidized surface area. ZJNM could adsorb on both the unoxidized surface area and oxidize surface area. On the unoxidized surface area, ZJNM adsorbed by forming Fe-S between S atoms on nanoparticles and Fe atoms on pyrite surface. On the oxidized surface area, ZJNM adsorbed through hydrogen bonding between -NH₂ on nanoparticles and Fe-OH on pyrite surface. Therefore, ZJNM was more effective collector than Y-89 for the flotation of pyrite in alkaline solution.

Acknowledgement

This work was financially funded by the Natural Science Foundation of Beijing Municipality (No. 2232083), Scientific Research Project for Overseas Students in Xiamen ([2022] 205), Jianlong Youth Scholar Funding (2023-1217), Fundamental Research Funds for the Central Universities (No. 00007733), and State Key Laboratory of Comprehensive Utilization of Low-Grade Refractory Gold Ores, Zijin Mining Group Co., Ltd.

References

ABÁNADES LÁZARO, ISABEL, ROSS S. FORGAN. 2019. 'Application of zirconium MOFs in drug delivery and biomedicine', *Coordination Chemistry Reviews*, 380: 230-59.

- AN, MAOYAN, YINFEI LIAO, XIAHUI GUI, YIFAN ZHAO, YUCHENG HE, ZECHEN LIU, QINGTENG LAI. 2020. *An investigation of coal flotation using nanoparticles as a collector*, International Journal of Coal Preparation and Utilization, 40: 679-90.
- BHARMORIA, PANKAJ, SÓNIA PM VENTURA. 2019. *Optical applications of nanomaterials*, Nanomaterials for Healthcare, Energy and Environment: 1-29.
- CHANG, HAIXIN, HONGKAI WU. 2013. *Graphene-based nanomaterials: Synthesis, properties, and optical and optoelectronic applications*, Advanced Functional Materials, 23: 1984-97.
- CHANG, ZIYONG, BAILI HE, XIAOSHA GONG, XIAOYUE QI, KEXIN LIU. 2023. *Cr-based metal-organic frameworks (MOFs) with high adsorption selectivity and recyclability for Au (III): Adsorption behavior and mechanism study*, Separation and Purification Technology, 325: 124612.
- CHANG, ZIYONG, FANGXU LI, XIAOYUE QI, BO JIANG, JUE KOU, CHUNBAO SUN. 2020. *Selective and efficient adsorption of Au (III) in aqueous solution by Zr-based metal-organic frameworks (MOFs): An unconventional way for gold recycling*, Journal of Hazardous Materials, 391: 122175.
- CHEN, JIANHUA, YUQIONG LI, CUIHUA ZHAO. 2014. *First principles study of the occurrence of gold in pyrite*, Computational Materials Science, 88: 1-6.
- CILEK, EMIN CAFER, SEVGI KARACA. 2015. *Effect of nanoparticles on froth stability and bubble size distribution in flotation*, International Journal of Mineral Processing, 138: 6-14.
- EKMEKÇI, Z., H. DEMIREL. 1997. *Effects of galvanic interaction on collectorless flotation behaviour of chalcopyrite and pyrite*, International Journal of Mineral Processing, 52: 31-48.
- HOFSTRA, ALBERT H, JEAN S CLINE. 2000. *Characteristics and models for Carlin-type gold deposits*.
- JARIWALA, DEEP, VINOD K SANGWAN, LINCOLN J LAUHON, TOBIN J MARKS, MARK C HERSAM. 2013. *Carbon nanomaterials for electronics, optoelectronics, photovoltaics, and sensing*, Chemical Society Reviews, 42: 2824-60.
- JIANG, C. L., X. H. WANG, B. K. PAREKH, J. W. LEONARD. 1998. *The surface and solution chemistry of pyrite flotation with xanthate in the presence of iron ions*, Colloids and Surfaces A: Physicochemical and Engineering Aspects, 136: 51-62.
- KASYMOVA, DIANA. 2019. *Carbon footprint of gold recovery from refractory ore in Russia*.
- LI, LI, PIN MA, SABIR HUSSAIN, LIANJUN JIA, DI LIN, XIONG YIN, YUAN LIN, ZHIHAI CHENG, LEYU WANG. 2019. *FeS₂/carbon hybrids on carbon cloth: a highly efficient and stable counter electrode for dye-sensitized solar cells*, Sustainable Energy & Fuels, 3: 1749-56.
- LIN, SHANGYONG, CHENGWEN WANG, RUNQING LIU, WEI SUN, GAOGUI JING. 2022. *Surface characterization of molybdenite, bismuthinite, and pyrite to identify the influence of pH on the mineral floatability*, Applied Surface Science, 577: 151756.
- LIU, KEXIN, HAO WANG, FENGYUAN ZHU, ZIYONG CHANG, RAN DU, YULIN DENG, XIAOYUE QI. 2024. *Lab on the Microneedles: A Wearable Metal-organic Frameworks-Based Sensor for Visual Monitoring of Stress Hormone*, ACS Nano, 18: 14207-17.
- MOHAMMADI-JAM, S, AD KE WATERS. 2016. *Inverse gas chromatography analysis of minerals: Pyrite wettability*, Minerals Engineering, 96: 130-34.
- MURGA, ROMINA, CAMILA RODRIGUEZ, JOHN AMALRAJ, DENNIS VEGA-GARCIA, LEOPOLDO GUTIERREZ, LINA URIBE. 2022. *Use of Polystyrene Nanoparticles as Collectors in the Flotation of Chalcopyrite*, Polymers, 14: 5259.
- NIU, XIAOPENG, JIANHUA CHEN, YUQIONG LI, LIUYIN XIA, LI LI, HEYUN SUN, RENMAN RUAN. 2019. *Correlation of surface oxidation with xanthate adsorption and pyrite flotation*, Applied Surface Science, 495: 143411.
- RAHMANI, ALI, MAHDI GHARABAGHI, HADI ABDOLLAHI. 2024. *Investigation of calcite flotation by green natural hydrophobic talc nanoparticles as collectors, and the adverse influence of nanoparticle aggregates*, Journal of Cleaner Production, 456: 142342.
- RIEDO, E., F. COMIN, J. CHEVRIER, F. SCHMITHUSEN, S. DECOSSAS, M. SANCROTTI. 2000. *Structural properties and surface morphology of laser-deposited amorphous carbon and carbon nitride films*, Surface and Coatings Technology, 125: 124-28.
- SHEN, PEILUN, DIANWEN LIU, XIAOLIN ZHANG, XIAODONG JIA, KAIWEI SONG, DAN LIU. 2019. *Effect of (NH₄)₂SO₄ on eliminating the depression of excess sulfide ions in the sulfidization flotation of malachite*, Minerals Engineering, 137: 43-52.

- SOBOUTI, ARASH, BAHRAM REZAI, FATEMEH SADAT HOSEINIAN. 2023. *A review of the application of nanoparticles as collectors in ion flotation*, *Physicochemical Problems of Mineral Processing*, 59.
- SUN, SHIOU-CHUAN. 1946. *Correlation between mineral behavior in cataphoresis and in flotation*.
- TAWADE, BHAUSAHEB V, IKEOLUWA E APATA, MANINDERJEET SINGH, PRIYANKA DAS, NIHAR PRADHAN, ABDULLAH M AL-ENIZI, ALAMGIR KARIM, DHARMARAJ RAGHAVAN. 2021. *Recent developments in the synthesis of chemically modified nanomaterials for use in dielectric and electronics applications*, *Nanotechnology*, 32: 142004.
- VAZIRI HASSAS, BEHZAD, HIDAYET CALISKAN, ONUR GUVEN, FIRAT KARAKAS, MUSTAFA CINAR, MEHMET S. CELIK. 2016. *Effect of roughness and shape factor on flotation characteristics of glass beads*, *Colloids and Surfaces A: Physicochemical and Engineering Aspects*, 492: 88-99.
- WANG, L., Y. PENG, K. RUNGE, D. BRADSHAW. 2015. *A review of entrainment: Mechanisms, contributing factors and modelling in flotation*, *Minerals Engineering*, 70: 77-91.
- YANG, SONGTAO, ROBERT PELTON. 2011. *Nanoparticle Flotation Collectors II: The Role of Nanoparticle Hydrophobicity*, *Langmuir*, 27: 11409-15.
- YANG, SONGTAO, ROBERT PELTON, MILES MONTGOMERY, YUGUO CUI. 2012. *Nanoparticle Flotation Collectors III: The Role of Nanoparticle Diameter*, *ACS Applied Materials & Interfaces*, 4: 4882-90.
- YANG, SONGTAO, ROBERT PELTON, ADAM RAEGEN, MILES MONTGOMERY, KARI DALNOKI-VERESS. 2011. *Nanoparticle Flotation Collectors: Mechanisms Behind a New Technology*, *Langmuir*, 27: 10438-46.
- YIN, WANZHONG, JIWEI XUE, DONG LI, QIANYU SUN, JIN YAO, SHI HUANG. 2018. *Flotation of heavily oxidized pyrite in the presence of fine digenite particles*, *Minerals Engineering*, 115: 142-49.
- ZHANG, HONGLIANG, QIQI ZHOU, SHANGYONG LIN, CHENYANG ZHANG, WEI SUN, DAIXIONG CHEN, RONG WANG, MENGFEI LIU, JIANHUA CHEN. 2022. *Surface modification of malachite with tetraamminecopper (II) and its effect on sulfidation flotation*, *Minerals Engineering*, 189: 107882.